Numerical Simulation of Fragment-Type Antenna by Using Finite Difference Time Domain (FDTD)

Li-Xia Yang, Xiao-Dong Ding, Da-Wei Ding[*], and Jing Xia

Abstract—Finite Difference Time Domain (FDTD) method is widely used in the simulation of various kinds of antennas. In this paper, research on the numerical simulation of the fragment-type antenna by using FDTD is conducted. The fragment-type antenna structures with different cell sizes and different overlapping sizes are simulated and measured. The validity of the numerical simulation of the fragment-type antenna by using FDTD is verified through the comparison between the simulated and measured return losses. In addition, its efficiency in terms of computation time shows great potential in engineering applications, especially when the design matrix is large enough.

1. INTRODUCTION

Fragment-type structure has found many successful applications in the antenna field [1–5]. In [1, 2], a fragment-type structure is utilized to design broadband and dual-band microstrip antennas. A circular polarization microstrip antenna is designed by employing a fragment-type structure in [3]. In [4], the concept of fragment-type structure is introduced to design a reconfigurable antenna. Compact fragment-type antenna is shown in [5].

Compared with the antennas with regular structures, a fragment-type antenna can be designed with higher filling efficiency and more design freedom in a given design region. Therefore, fragment-type structure is promising for compact antenna, antenna with novel structure, and antenna with higher electrical performance.

It is well known that a fragment-type antenna is mainly optimized by using evolutionary algorithms (EAs), such as Genetic Algorithm (GA) [6] and Multiobjective Evolutionary Algorithm Based on Decomposition combined with Enhanced Genetic Operators (MOEA/D-GO) [7]. In these EAs, fitness evaluation is necessary, which corresponds to simulation of the electrical parameters of a fragment-type antenna. There are some candidates for the stimulation of a fragment-type antenna, such as Computer Simulation Technology (CST) [8], High Frequency Structure Simulator (HFSS) [9], and FDTD Simulation software (XFDTD) [10]. However, those methods are extremely computationally expensive. Finite Difference Time Domain (FDTD) source code becomes an excellent solution because of its following features,

1) it is easy to obtain electrical characteristics over broadband through a single run in time domain,
2) those cells of the fragment-type structure can be consistent with the generated cells in the FDTD implement, and
3) parallel version of FDTD has been widely used.

Although FDTD source code has been used for numerical simulation of fragment-type antennas [11, 12], there is no work on investigating the numerical simulation of fragment-type antennas with different cell sizes and different overlapping dimensions. Moreover, there is no research on validating its efficiency when the design matrix of the fragment-type structure is large enough.

This paper simulates a fragment-type antenna by using FDTD method, studies the influence of different cell sizes and overlapping sizes on the simulation results, and verifies the high efficiency of FDTD through the comparison among the simulation results.

The paper is organized as follows. The algorithm principle of FDTD is reviewed simply in Section 2. Fragment-type structure and its simulation by using FDTD are demonstrated in Section 3. In Section 4, we study the simulated and measured results of the fragment-type antenna structures with different cell sizes and overlapping sizes. In Section 5, a conclusion and prospect for the research work of this paper is presented.

2. FDTD PRINCIPLE

2.1. Governing Equations

FDTD method starts from the differential form of Maxwell's two curl equations as shown in Eqs. (1) and (2). To keep it simple in this article, the media are assumed to be lossless and isotropic. On the basis of these assumptions, Maxwell's curl equations may be written as

$$\nabla \times E = -\frac{\partial B}{\partial t} - J_m \tag{1}$$

$$\nabla \times H = \frac{\partial D}{\partial t} + J \tag{2}$$

where E, H, D and B represent electric field intensity, magnetic field intensity, electric flux density, and magnetic flux density, respectively. J and J_m represent electric current density and equivalent magnetic current density. The finite difference approximations to Eqs. (1) and (2) are

$$
\begin{aligned}
E_{xi+1/2,j,k}^{n+1} =& \left(\frac{1 - \dfrac{\sigma_{i+1/2,j,k}\Delta t}{2\varepsilon_{i+1/2,j,k}}}{1 + \dfrac{\sigma_{i+1/2,j,k}\Delta t}{2\varepsilon_{i+1/2,j,k}}} \right) \cdot E_{xi+1/2,j,k}^{n} + \left(\frac{\dfrac{\Delta t}{\varepsilon_{i+1/2,j,k}}}{1 + \dfrac{\sigma_{i+1/2,j,k}\Delta t}{2\varepsilon_{i+1/2,j,k}}} \right) \\
&\cdot \left(\frac{H_{zi+1/2,j+1/2,k}^{n+1/2} - H_{zi+1/2,j-1/2,k}^{n+1/2}}{\Delta y} - \frac{H_{yi+1/2,j,k+1/2}^{n+1/2} - H_{yi+1/2,j,k-1/2}^{n+1/2}}{\Delta z} \right)
\end{aligned} \tag{3}
$$

$$
\begin{aligned}
E_{yi,j+1/2,k}^{n+1} =& \left(\frac{1 - \dfrac{\sigma_{i,j+1/2,k}\Delta t}{2\varepsilon_{i,j+1/2,k}}}{1 + \dfrac{\sigma_{i,j+1/2,k}\Delta t}{2\varepsilon_{i,j+1/2,k}}} \right) \cdot E_{yi,j+1/2,k}^{n} + \left(\frac{\dfrac{\Delta t}{\varepsilon_{i,j+1/2,k}}}{1 + \dfrac{\sigma_{i,j+1/2,k}\Delta t}{2\varepsilon_{i,j+1/2,k}}} \right) \\
&\cdot \left(\frac{H_{xi,j+1/2,k+1/2}^{n+1/2} - H_{xi,j+1/2,k-1/2}^{n+1/2}}{\Delta z} - \frac{H_{zi+1/2,j+1/2,k}^{n+1/2} - H_{zi-1/2,j+1/2,k}^{n+1/2}}{\Delta x} \right)
\end{aligned} \tag{4}
$$

$$
\begin{aligned}
E_{zi,j,k+1/2}^{n+1} =& \left(\frac{1 - \dfrac{\sigma_{i,j,k+1/2}\Delta t}{2\varepsilon_{i,j,k+1/2}}}{1 + \dfrac{\sigma_{i,j,k+1/2}\Delta t}{2\varepsilon_{i,j,k+1/2}}} \right) \cdot E_{zi,j,k+1/2}^{n} + \left(\frac{\dfrac{\Delta t}{\varepsilon_{i,j,k+1/2}}}{1 + \dfrac{\sigma_{i,j,k+1/2}\Delta t}{2\varepsilon_{i,j,k+1/2}}} \right) \\
&\cdot \left(\frac{H_{yi+1/2,j,k+1/2}^{n+1/2} - H_{yi-1/2,j,k+1/2}^{n+1/2}}{\Delta x} - \frac{H_{xi,j+1/2,k+1/2}^{n+1/2} - H_{xi,j-1/2,k+1/2}^{n+1/2}}{\Delta y} \right)
\end{aligned} \tag{5}
$$

$$H_{xi,j+1/2,k+1/2}^{n+1/2} = \left(\frac{1 - \frac{\sigma_{i,j+1/2,k+1/2}\Delta t}{2\mu_{i,j+1/2,k+1/2}}}{1 + \frac{\sigma_{i,j+1/2,k+1/2}\Delta t}{2\mu_{i,j+1/2,k+1/2}}} \right) \cdot H_{xi,j+1/2,k+1/2}^{n-1/2} + \left(\frac{\frac{\Delta t}{\mu_{i,j+1/2,k+1/2}}}{1 + \frac{\sigma_{i,j+1/2,k+1/2}\Delta t}{2\mu_{i,j+1/2,k+1/2}}} \right)$$

$$\cdot \left(\frac{E_{zi,j+1,k+1/2}^{n} - E_{zi,j,k+1/2}^{n}}{\Delta y} - \frac{E_{yi,j+1/2,k+1}^{n} - E_{yi,j+1/2,k}^{n}}{\Delta z} \right) \tag{6}$$

$$H_{yi+1/2,j,k+1/2}^{n+1/2} = \left(\frac{1 - \frac{\sigma_{i+1/2,j,k+1/2}\Delta t}{2\mu_{i+1/2,j,k+1/2}}}{1 + \frac{\sigma_{i+1/2,j,k+1/2}\Delta t}{2\mu_{i+1/2,j,k+1/2}}} \right) \cdot H_{yi+1/2,j,k+1/2}^{n-1/2} + \left(\frac{\frac{\Delta t}{\mu_{i+1/2,j,k+1/2}}}{1 + \frac{\sigma_{i+1/2,j,k+1/2}\Delta t}{2\mu_{i+1/2,j,k+1/2}}} \right)$$

$$\cdot \left(\frac{E_{xi+1/2,j,k+1}^{n} - E_{xi+1/2,j,k}^{n}}{\Delta z} - \frac{E_{zi+1,j,k+1/2}^{n} - E_{zi,j,k+1/2}^{n}}{\Delta x} \right) \tag{7}$$

$$H_{zi+1/2,j+1/2,k}^{n+1/2} = \left(\frac{1 - \frac{\sigma_{i+1/2,j+1/2,k}\Delta t}{2\mu_{i+1/2,j+1/2,k}}}{1 + \frac{\sigma_{i+1/2,j+1/2,k}\Delta t}{2\mu_{i+1/2,j+1/2,k}}} \right) \cdot H_{zi+1/2,j+1/2,k}^{n-1/2} + \left(\frac{\frac{\Delta t}{\mu_{i+1/2,j+1/2,k}}}{1 + \frac{\sigma_{i+1/2,j+1/2,k}\Delta t}{2\mu_{i+1/2,j+1/2,k}}} \right)$$

$$\cdot \left(\frac{E_{yi+1,j+1/2,k}^{n} - E_{yi,j+1/2,k}^{n}}{\Delta x} - \frac{E_{xi+1/2,j+1,k}^{n} - E_{xi+1/2,j,k}^{n}}{\Delta y} \right) \tag{8}$$

where Δx, Δy and Δz represent the sizes along three directions of each unit cell, respectively, and Δt represents the time step. σ, ε and μ represent electric conductivity, electrical permittivity and magnetic permeability, respectively. i, j and k correspond to the node numbers of the unit cell in the $\hat{x}$, $\hat{y}$ and $\hat{z}$ directions.

2.2. Courant Stability Condition

Due to the numerical dispersion in the above approximations, the maximum time steps that may be used are limited

$$c\Delta t \leq \frac{1}{\sqrt{\frac{1}{(\Delta x)^2} + \frac{1}{(\Delta y)^2} + \frac{1}{(\Delta z)^2}}} \tag{9}$$

2.3. Source Consideration

In this paper, a Gaussian pulse is considered as the excitation because it will provide frequency-domain information from dc to the desired cutoff frequency by adjusting the width of the pulse. For a more intuitive representation, the computational model is shown in Fig. 1. The vertical electric field is imposed in order to simulate a voltage source excitation. The time-domain form of Gaussian pulse can be expressed as

$$E_i(t) = 0.5 * \exp\left(-\frac{(t - t_0)^2}{\tau^2} \right) \tag{10}$$

where τ is constant, which determines the width of the Gaussian pulse. t_0 is the moment of pulse peak. Because the antenna used in this paper works in $2\,\text{GHz}$–$20\,\text{GHz}$, we set $\tau = 25\,\text{ps}$, $t_0 = 150\,\text{ps}$.

2.4. Input Resistance

After all transients have been finished, electric and magnetic field components are solved, and then the transient voltage and current can be obtained. The transient voltage and current are reached by using
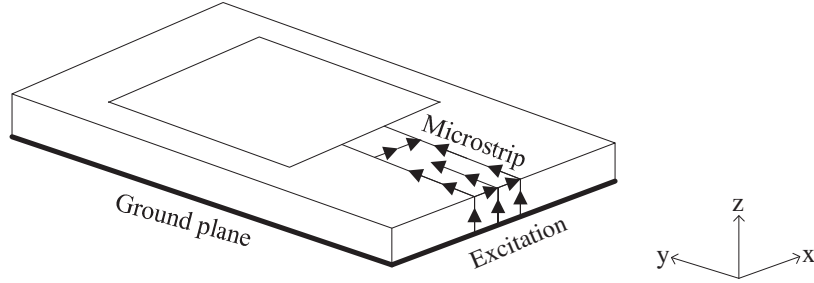
Figure 1. Computational model.

Fourier transform. The input impedance can be obtained as

$$Z_{in} = \frac{U_z}{I_z} \tag{11}$$

where U_z and I_z are the frequency responses of the transient voltage and current.

Then the reflection coefficient can be determined according to the formula

$$S_{11} \, (\text{dB}) = 20 \lg \left| \frac{Z_{in} - Z_c}{Z_{in} + Z_c} \right| \tag{12}$$

where Z_c is the characteristic impedance, and it should be noted that the reference plane is different form the feed plane, which is chosen with enough distance from the circuit discontinuities to eliminate evanescent waves.

2.5. Absorbing Boundary

Due to the finite capabilities of the computer used to calculate the finite-difference equations, the mesh must be limited in the $\hat{x}$, $\hat{y}$ and $\hat{z}$ directions. Nearly Perfectly Matched Layer (NPML) proposed by Cummer [13] serves as absorption boundary in this paper because of its simplify for programming while maintaining the same absorbing ability as Perfectly Matched Layer. For the stability of calculation, we set the thickness of NPML as 6 grids to eliminate the reflection of electromagnetic waves appearing at the truncated mesh.

3. MICROSTRIP ANTENNA CONFIGURATION

3.1. Fragment-type Structure

In a fragment-type structure, design space is dispersed into cells assigned with "1" or "0", where cells assigned with "1" are to be metalized, as shown in Fig. 2. The distribution of "1" and "0" forms a two-dimensional (2D) 0/1 design matrix and can be used for optimization design, such as isolation, gain, beam pattern, bandwidth in [14].
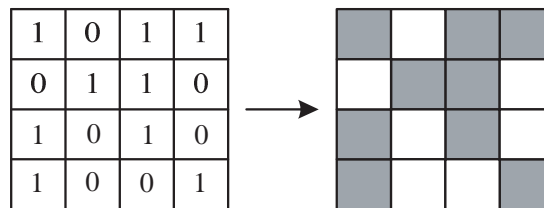

Figure 2. Fragment-type structure and its design matrix.

3.2. Simulation of the Fragment-Type Structure Antenna by Using FDTD

This paper focuses on the microstrip antenna with a fragment-type structure as shown in Fig. 3, which is printed on a Duroid 5880 substrate ($15.6\,\text{mm} \times 33.6\,\text{mm} \times 0.794\,\text{mm}$) with relative dielectric constant of 2.2. The antenna consists of a rectangular patch ($L_1 \times L_2 = 16.0\,\text{mm} \times 12\,\text{mm}$) and a microstrip feedline ($L_3 \times L_4 = 2.40\,\text{mm} \times 16.00\,\text{mm}$), where the distance between the feedline and the edge of the patch is $L_5 = 2.00\,\text{mm}$. The only difference between this structure and the one in [15] is that we take a fragmented discretization for the rectangular radiation patch.
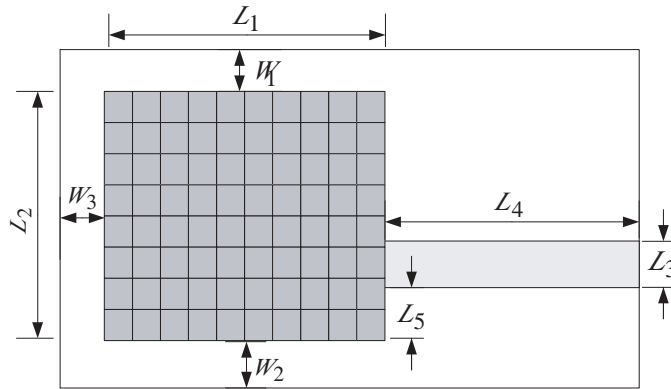

Figure 3. Antenna configuration.

This paper selects $\Delta x = 0.2\,\text{mm}$, $\Delta y = 0.2\,\text{mm}$, $\Delta z = 0.1985\,\text{mm}$, and time interval is set as $\Delta t = 0.0331\,\text{ps}$ according to the stability conditions. The simulated antennas all have the same spatial step and time interval. Therefore, the rectangular radiation patch can be divided into $60\Delta x \times 80\Delta y$ cells, and the distances between the edge of the patch and the edge of the substrate are $W_1 = W_2 = 8\Delta x$ and $W_3 = 8\Delta y$, respectively. The dimensions of the feedline are $L_3 = 12\Delta x$ and $L_4 = 80\Delta y$. In this design, the size of each metallic element is $L_c \times L_d$. The sub-patches overlap with the size of $L_a \times L_b$ to ensure electrical contact in such constellations in fabricated antenna [16]. The overlapped elements are shown in Fig. 4. It shall be noted that different cell sizes and overlapping sizes have certain influence on the electrical performance of the fragment-type antenna.
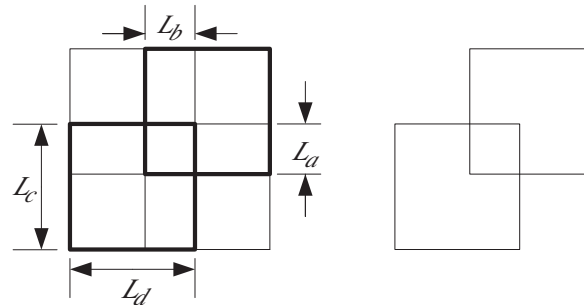

Figure 4. Geometry of the overlapping element.

4. SIMULATION RESULTS

In this section, we first study the simulation results of the fragment-type structure antenna with different cell sizes, i.e., 3×4, 15×20 and 30×40. Then, we study the influence of different overlapping dimensions, i.e., $\Delta x \times \Delta y$, $2\Delta x \times 2\Delta y$ and $3\Delta x \times 3\Delta y$, respectively, on the simulation results.

4.1. Different Cell Sizes

Firstly, the rectangular patch can be divided into 3×4 cells. The dimensions of each element are $L_c = 20\Delta x$ and $L_d = 20\Delta y$, and the size of the overlapping cell is $L_a \times L_b = \Delta x \times \Delta y$. The simulation is performed for 10000 time steps. Fig. 5(a) shows a fragment-type antenna generated randomly. The prototype of this design is fabricated as shown in Fig. 5(b), and the simulated and measured results are illustrated in Fig. 5(c). From Fig. 5(c), it is clearly observed that agreement between numerical results is good. The slight difference between the simulated and measured results is believed to be caused by the fabrication and measurement error.
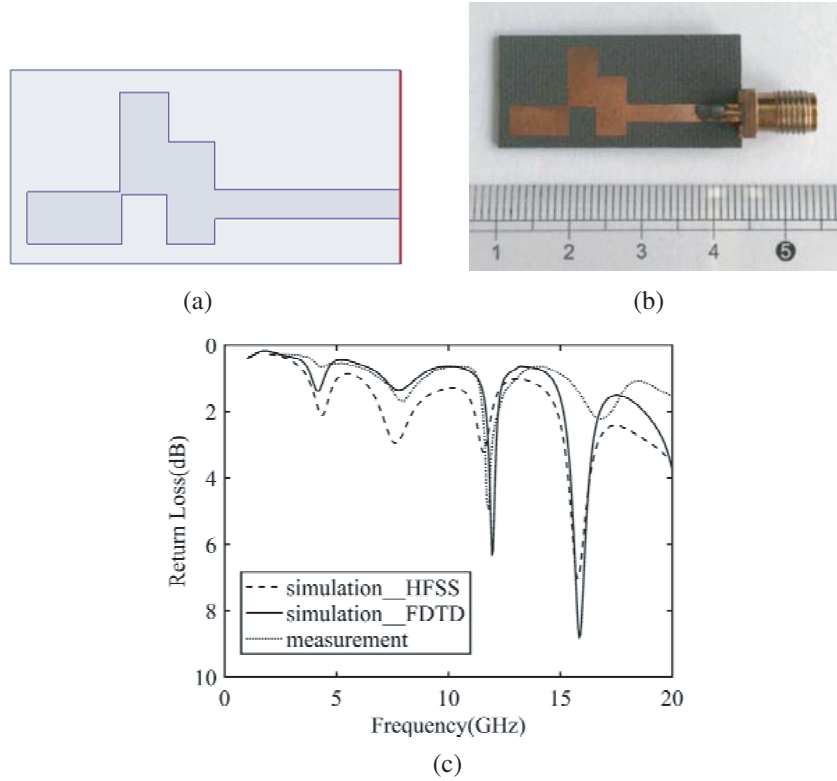

(a)

(b)

(c)

Figure 5. Simulated and measured results of antenna divided into 3×4 cells. (a) Antenna structure, (b) photograph of the fabricated antenna, and (c) comparison of numerical results.

Secondly, the rectangular patch is divided into 15×20 cells. The dimensions of each element are $L_c = 4\Delta x$ and $L_d = 4\Delta y$, and the size of overlapping cell is $L_a \times L_b = \Delta x \times \Delta y$, as time steps shall be set as 10000. Fig. 6(a) provides a set of design model generated randomly. The prototype of this design is fabricated as shown in Fig. 6(b), and the numerical results are shown in Fig. 6(c). At this point, compared with the simulated result which is realized by means of the simulation of HFSS, slight frequency offset may exist in the numerical result realized by using FDTD. However, they are both in a similar trend. The slight difference between the simulated and measured results is believed to be caused by the fabrication and measurement error.

Then, we disperse rectangular patch into 30×40 cells. The dimensions of each element are $L_c = 2\Delta x$ and $L_d = 2\Delta y$, and the size of the overlapping cell is still $L_a \times L_b = \Delta x \times \Delta y$. The simulation is performed for 10000 time steps. Fig. 7(a) provides a fragment-type antenna generated randomly. The prototype of this design is also fabricated as shown in Fig. 7(b). Fig. 7(c) shows the stimulated and measured results. Compared with the simulated result which is realized by means of the simulation of HFSS, the numerical result realized by using FDTD still has slight frequency offset, especially at high frequency. The difference between the simulated and measured results is believed to be caused by the fabrication and measurement error.
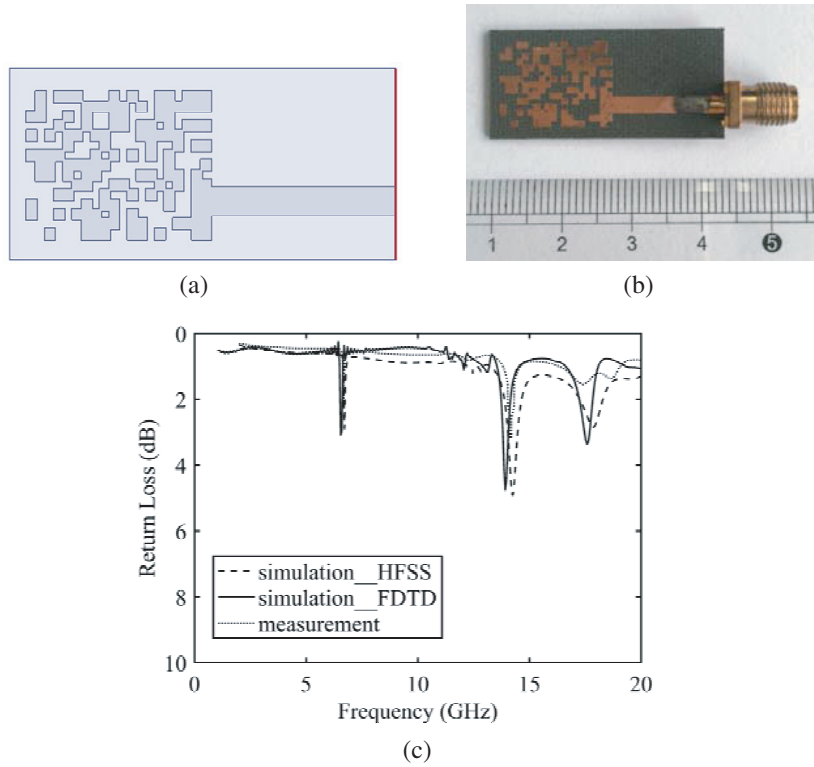
(a)

(b)

(c)

Figure 6. Simulated and measured results of antenna divided into 15×20 cells. (a) Antenna structure, (b) photograph of the fabricated antenna, and (c) comparison of numerical results.
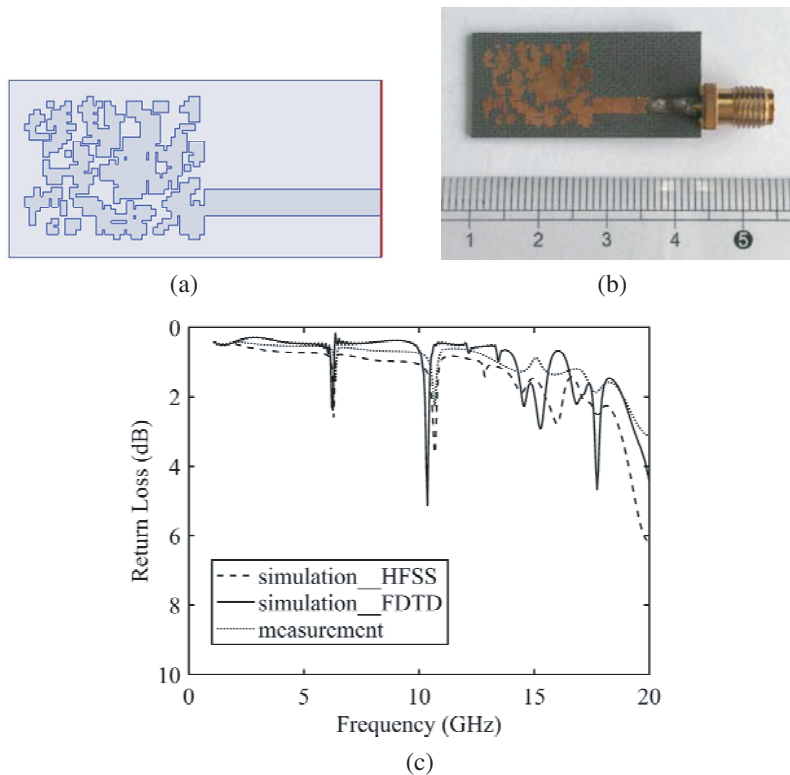

(a)

(b)

(c)

Figure 7. Simulated and measured results of antenna divided into 30×40 cells. (a) Antenna structure, (b) photograph of the fabricated antenna, and (c) comparison of numerical results.

Seen from the simulated results of above three antenna structures with different cell sizes, we can find that the fewer the cells are, the higher the precision is. Both of the simulated results obtained through FDTD and HFSS have certain errors, because

1) there are many irregular structures and parasitic elements in the fragment-type structures, which may cause serious current oscillation, so that energy cannot be radiated or reflected completely within finite time steps,

2) numerical errors from the simulation of FDTD, such as the exclusion of dielectric and conductor loss in the FDTD calculation. This will cause the calculated S parameters shifting up at the higher frequencies. Meanwhile, the modeling error occurs primarily in the inability to match all of the circuit dimensions, and

3) numerical errors from the simulation of HFSS, such as the size of air box and dielectric loss of the substrate.

Table 1 exhibits the computation cost corresponding to the above designs using HFSS and FDTD. It is demonstrated that the high efficiency of the simulation by using FDTD is obvious when design matrix is large enough, which is useful for practical engineering applications.

Table 1. Comparison of time consumption. (Units: minute).

Design	HFSS			FDTD
	Model	Calculation	Total time	Total time
I	4.5	0.7	5.2	4.8
II	5.2	1.2	6.4	5.2
III	7.1	3.2	10.3	5.6

4.2. Different Overlapping Sizes

The influence of the different overlapping sizes is discussed in this section. The antenna structure with the radiation patch divided into 3×4 cells in Section 3.1 is used for comparison. The simulated results under the three circumstances are presented in Fig. 8. As can be seen, in this antenna structure, when the size of the overlapping cell is $L_a \times L_b = 3\Delta x \times 3\Delta y$, compared with the simulated result realized by means of the simulation of HFSS, the numerical result realized by using FDTD is the most consistent. Therefore, it is concluded that different overlapping sizes will affect the accuracy of the numerical simulation. Therefore, in the practical engineering application, the overlapping size is of certain research significance.
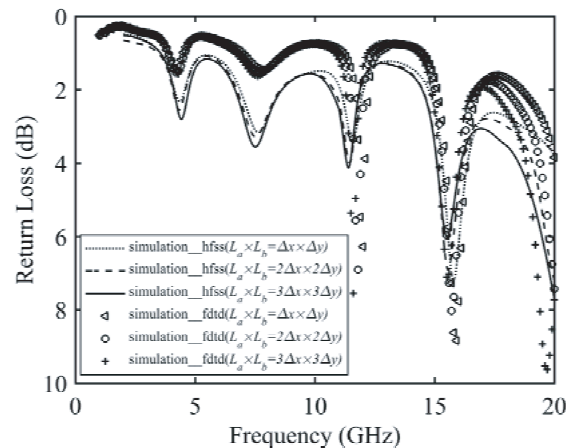

Figure 8. Simulated results of antenna with different overlapping size.

5. CONCLUSIONS

The return loss of the fragment-type structure by using FDTD is calculated in this paper. The numerical results of the fragment-type antenna structures with different cell sizes and overlapping sizes are discussed. The validity of the numerical simulation of the fragment-type antenna by using FDTD is verified through the comparison between the simulated and measured return losses. Meanwhile, its efficiency in terms of computation time shows great potential in engineering applications, especially when the design matrix is large enough.

ACKNOWLEDGMENT

REFERENCES

1. Choo, H. and H. Ling, "Design of broadband and dual-band microstrip antennas on a high-dielectric substrate using a genetic algorithm," *IEEE Transactions on Antennas and Propagation*, Vol. 150, No. 3, 137–142, Jun. 2003.
2. Choo, H., A. Hutani, and L. C. Trintinalia, "Shape optimisation of broadband microstrip antennas using genetic algorithm," *IET Electronics Letters*, Vol. 36, No. 25, 2057–2058, Dec. 2000.
3. Alatan, L., M. I. Aksun, and K. Leblebicioglu, "Use of computationally efficient method of moments in the optimization of printed antennas," *IEEE Transactions on Antennas and Propagation*, Vol. 47, No. 4, 725–732, Apr. 1999.
4. Pringle, L. N., P. H. Harms, and S. P. Blalock, "A reconfigurable aperture antenna based on switched links between electrically small metallic patches," *IEEE Transactions on Antennas and Propagation*, Vol. 52, No. 6, 1434–1445, Jun. 2004.
5. Soontornpipit, P., C. M. Furse, and C. C. You, "Miniaturized biocompatible microstrip antenna using genetic algorithm," *IEEE Transactions on Antennas and Propagation*, Vol. 53, No. 6, 1939–1945, Jun. 2005.
6. John, M. and M. J. Ammann, "Wideband printed monopole design using a genetic algorithm," *IEEE Antennas & Wireless Propagation Letters*, Vol. 6, No. 11, 447–449, Sep. 2007.
7. Ding, D. W. and G. Wang, "MOEA/D-GO for fragmented antenna design," *Progress In Electromagnetics Research*, Vol. 33, 1–5, Oct. 2013.
8. John, M. and M. J. Ammann, "Design of a wide-band printed antenna using a genetic algorithm on an array of overlapping sub-patches," *IEEE International Workshop on Antenna Technology Small Antennas and Novel Metamaterials*, 92–95, 2006.
9. Herscovici, N., J. Ginn, and T. Donisi, "A fragmented aperture-coupled microstrip antenna," *IEEE Antennas and Propagation Society International Symposium*, 1–4, San Diego, Jul. 2008.
10. Jin, Z., H. Yang, and X. Tang, "Parameters and schemes selection in the optimization of the fragment-type tag antenna," *Third International Joint Conference on Computational Science and Optimization IEEE Computer Society*, Vol. 2, 259–262, May 2010.
11. Goojo, K. and Y. C. Chung, "Optimization of UHF RFID tag antennas using a genetic algorithm," *IEEE Antennas and Propagation Society International Symposium*, 2087–2090, Jul. 9–14, 2006.
12. Jin, Z., H. Yang, X. Tang, and J. Mao, "Impedance analysis of the fragment-type tag antenna using FDTD," *International Symposium on Antennas, IEEE Transactions on Antennas and Propagation*, 260–262, Nov. 2008.
13. Cummer, S. A., "A simple, nearly perfectly matched layer for general electromagnetic media," *IEEE Microwave & Wireless Components Letters*, Vol. 13, No. 3, 128–130, Apr. 2003.

14. Johnson, J. M. and Y. Rahmat-Samii, "Genetic algorithms and method of moments (GA/MOM) for the design of integrated antennas," *IEEE Transactions on Antennas and Propagation*, Vol. 47, No. 10, 1606–1614, Oct. 1999.

15. Sheen, D. M., S. M. Ali, and M. D. Abouzahra, "Application of the three-dimensional finite-difference time-domain method to the analysis of planar microstrip circuits," *IEEE Transactions on Microwave Theory & Techniques*, Vol. 8, No. 7, 849–857, Jun. 1990.

16. Merulla, E. J. and R. Bansal, "Optimized design and fabrication of a fragmented wire antenna," *IEEE Sarnoff Symposium*, 1–4, Sarnoff, Apr. 28–30, 2008.